

# openTSNE: a modular Python library for t-SNE dimensionality reduction and embedding

Pavlin G. Poličar<sup>1</sup>  
pavlin.policar@fri.uni-lj.si

Martin Stražar<sup>2</sup>

Blaž Zupan<sup>1,3</sup>

<sup>1</sup>Faculty of Computer and Information Science, University of Ljubljana,  
Večna pot 113, SI-1000 Ljubljana, Slovenia

<sup>2</sup>Broad Institute of Harvard and MIT,  
Düsternbrooker Weg 20, MA-02142 Cambridge, U.S.A.

<sup>3</sup>Department of Molecular and Human Genetics, Baylor College of Medicine,  
1 Baylor Plaza, TX-77030 Houston, U.S.A.

## Abstract

Point-based visualizations of large, multi-dimensional data from molecular biology are often used to reveal meaningful clusters. One of the most popular techniques to construct such visualizations is *t*-distributed stochastic neighbor embedding (t-SNE). Several extensions of t-SNE have recently been proposed to address issues of scalability and the quality of the resulting visualizations. We introduce openTSNE, a modular Python library that implements the core t-SNE algorithm and its many extensions. The library is fast and enables users to embed data sets containing millions of data points in a matter of minutes on consumer-grade laptop computers. Unique to openTSNE is also the ability to map new data to existing embeddings, which can surprisingly assist in solving batch effects.

**Keywords** — t-SNE, embedding, visualization, dimensionality reduction, Python library

## Introduction

The abundance of high-dimensional data sets in molecular biology calls for dimensionality reduction techniques that are able to produce informative data visualizations. Popular approaches include principal component analysis (PCA), multidimensional scaling, t-distributed stochastic neighbor embedding (t-SNE) [1], and uniform manifold approximation and projections (UMAP) [2]. Among these, t-SNE has received much attention as it can address high volumes of data and reveal meaningful clustering structure. The increased resolution and throughput of modern molecular assays has lead to the frequent use of t-SNE in diverse fields including, but not limited to, single-cell transcriptomics (scRNA-seq, [3, 4, 5]), human genetics [6], metagenomic assembly [7], the spatial organization of microbial communities [8] and metabolomics [9]. Reports on single-cell gene expression data, our running example, often start with an overview of the cell landscape, where t-SNE is used to embed high-dimensional expression profiles into a two-dimensional space. Figs. 1.a and 1.b show two such embeddings.

Despite its utility, t-SNE has often been criti-

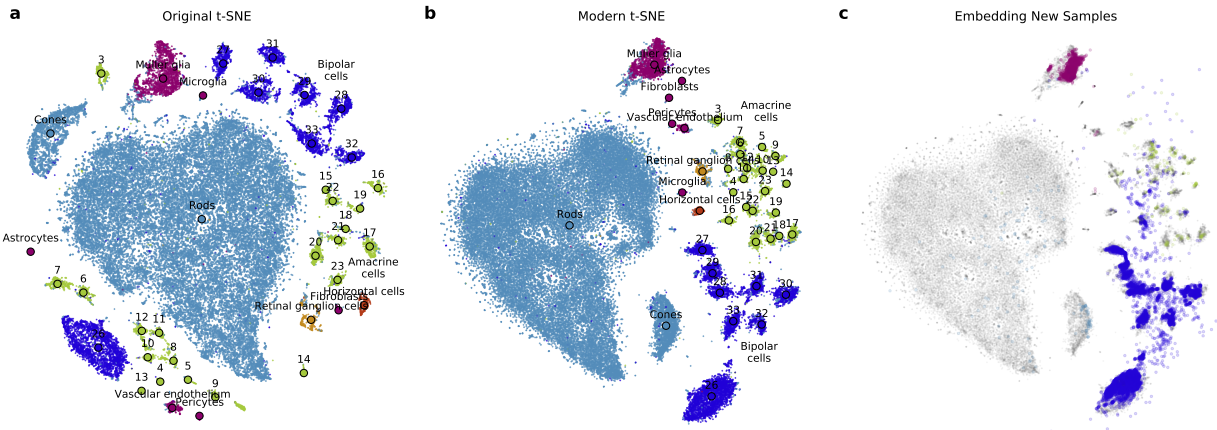


Figure 1: We use openTSNE to generate three t-SNE embeddings and demonstrate recent theoretical advances. The data in (a) and (b) represent 44,808 single-cell gene-expression profiles of mouse retinal cells from Macosko *et al.* [3]. The data in (c) additionally contains 27,499 expression profiles from mouse retinal cells from Shekhar *et al.* [10]. (a) We construct a t-SNE embedding following the parameter choices from the original publication by Maaten & Hinton [1]. The visualization shows no preservation of the global organization of clusters, resulting from random initialization and an affinity model focused on preserving local neighborhoods. (b) A modern t-SNE embedding, utilizing the latest theoretical advances and practical recommendations constructed using a multi-scale affinity model, preserving both short-range and long-range interactions between data points and initialized so that the global layout is as meaningful as possible. Unlike in (a), the green and blue clusters representing different sub-types of amacrine and bipolar cells are now localized to the same regions of the space, indicating a higher level of similarity than to other cell types. The embedding in (c) shows how existing t-SNE reference atlases can be used to place new samples into existing embeddings. The positions of new data points correspond to cell types from the reference atlas.

cized for its limited scalability, lack of global organization – t-SNE identifies well-defined clusters that may be arbitrarily scattered throughout the low-dimensional space – and the absence of theoretically-founded methods to map new data into existing embeddings [11, 12]. Most of these shortcomings have recently been addressed. Linderman *et al.* developed an interpolation-based approximation scheme which massively improved the scalability of t-SNE, achieving linear time complexity in the number of samples [13]. Kobak & Berens proposed several techniques to improve global cluster coherence, including estimating similarities with a mixture of Gaussian kernels [14]. In our previous work, we presented a principled approach for embedding new samples into existing visualizations [15].

## Results

We introduce `openTSNE`, a comprehensive Python library that implements t-SNE and all its recently proposed extensions, including:

1. the implementation of efficient approximation schemes [16, 13] allowing the embedding of millions of data points,
2. the addition of new data samples into a fixed existing embeddings [15],
3. improved initialization schemes [17] leading to more globally consistent layouts,
4. variable degrees of freedom [18] allowing the inspection of data at different levels of resolution,
5. multi-scale similarity kernels [14] which preserve small, well-defined clusters and uncover global relationships between clusters, and
6. improved defaults for learning rate and number of iterations [19] which produce embeddings at a lower computational cost.

`openTSNE` is compatible with the Python data science ecosystem and libraries including `numpy`, `scikit-learn`, `scipy`), providing a familiar and intuitive application program interface to new users. Its modu-

lar design encourages extensibility and experimentation with various settings and changes to the analysis pipeline. We have released `openTSNE` to the open-source community to make recent theoretical advancements more accessible to a wider audience. At the time of the writing, the library averages thousands of weekly downloads and has received almost 700 GitHub stars, an appreciation score gained by only 0.3% of public Python repositories. The source code is available at <https://github.com/pavlin-policar/openTSNE> and supports installations from PyPI and conda-forge, the two most widely adopted Python package managers.

Accessibility of the latest theoretical advancements in t-SNE is one of the core design principles of `openTSNE`. This range of advancements is easily accessible through an intuitive programming interface, where we closely follow the style `scikit-learn` [20], a popular and widely used library for machine learning. The following snippet exemplifies this interface and was used to generate the four visualizations in Fig. 2, demonstrating the effect of a particular recent theoretical advancements in the t-SNE algorithm.

---

```
import openTSNE
from openTSNE.affinity import Multiscale
# a - standard t-SNE
tsne1 = openTSNE.TSNE(perplexity=30).fit(X)
# b - high perplexity for global structure
tsne2 = openTSNE.TSNE(perplexity=500).fit(X)
# c - multiscale kernel for local/global structure
aff = Multiscale(X, perplexities=[30, 500])
tsne3 = openTSNE.TSNE(affinities=aff).fit(X)
# d - decrease dof for higher resolution
tsne4 = openTSNE.TSNE(dof=0.6).fit(X)
```

---

The code snippet considers a `numpy` array or `scipy` sparse matrix `X` and creates four `TSNEEmbedding` objects. These objects represent t-SNE embeddings that may subsequently be optimized under different parameter settings or used to embed new samples into the embedding landscape. Function calls may include additional parameters not shown in the example code but are explained in the accompanying notebooks available at <https://github.com/pavlin-policar/opentsne-paper>.

## Discussion

### Uncovering Structure in High-Dimensional Data

Dimensionality reduction techniques implicitly assume that high-dimensional data lies on a lower-dimensional manifold, which can accurately be captured by a small number of dimensions. However, there is no evidence that every data set can accurately be described using only two dimensions, and any such embedding will inevitably lead to a loss of information. Thus, it is beneficial to examine multiple embeddings, each of which provides a different perspective on topology and other data characteristics.

We illustrate this point by generating four different embeddings of the data on single-cell gene expression in mouse brain [5]. Fig. 2.a shows an embedding using default t-SNE parameters. While different clusters of excitatory and inhibitory neurons appear close to one another, all clusters appear equidistant from their neighbors, and the overall relations between groups are not obvious. The embedding in Fig. 2.b focuses on preserving larger neighborhoods of points, resulting in a more globally consistent layout where relations between clusters become more apparent. Here, it is evident from the increased white space between groups that there is one large class of excitatory neurons and two related classes of inhibitory neurons. Unfortunately, focusing on preserving large neighborhoods leads to the absorption of smaller clusters into larger ones. Alternatively, Fig. 2.c uses multi-scale similarity kernels that aim to preserve both the global organization of clusters and prevent smaller cluster absorption. We constructed the embedding from Fig. 2.d with the settings used for Fig. 2.a, but at a finer level of resolution. The figure demonstrates that some clusters are composed of numerous, smaller subgroups representing different cell subpopulations which are not visible under standard parameter settings.

When dealing with data containing millions of data points, standard t-SNE embeddings often become unwieldy – cluster boundaries are blurred, large clusters absorb smaller ones, and relationships between clus-

ters become increasingly difficult to interpret. We constructed Fig. 3.a from the data containing expression profiles of over two million single cells captured at different time points in mouse development. The embedding indicates numerous clusters with transitions between time points, as marked by the color-coding, that are difficult to interpret. Kobak & Berens observed that increasing attractive forces between similar data points controlled via the *exaggeration* parameter leads to more compact clusters, and subsequently, more informative visualizations [14]. For instance, 3.b doubles the default exaggeration, which uncovers some of the data’s overall structure. Further doubling the exaggeration in 3.c allows us to observe that the data is comprised of two main groups of cells and eight somewhat smaller clusters. The visualization also reveals several tiny clusters, possibly corresponding to rare cell types.

Exaggeration can highlight transitions between cell states in developmental studies. Standard t-SNE often produces embeddings with clearly defined, discrete clusters. We can adjust the level of granularity and resolution of the clusters with several parameters in Fig. 2. However, discrete clusters are often undesired in developmental studies where cells’ state is assumed to follow a continuous transition path. To this end, other embedding techniques such as UMAP and ForceAtlas2 [21] are used to better capture the continuity between cell states. Recently, Böhm *et al.* [22] showed that embeddings produced by t-SNE with exaggeration values of 4 and  $\sim 30$  construct embeddings which are markedly similar to UMAP and ForceAtlas2, respectively. For example, in Fig. 3.a, the developmental trajectory between different time points is difficult to observe due to many sprawled out clusters. On the other hand, it is easier to trace the development when we increase the exaggeration factor from 1 to 2 to 4 in Figs. 3.b-c.

### Embedding New Samples

Unlike other popular dimensionality reduction techniques such as principal component analysis or autoencoders, t-SNE is a non-parametric method and does not define an explicit mapping to the embedding space. Therefore embeddings of new data points need

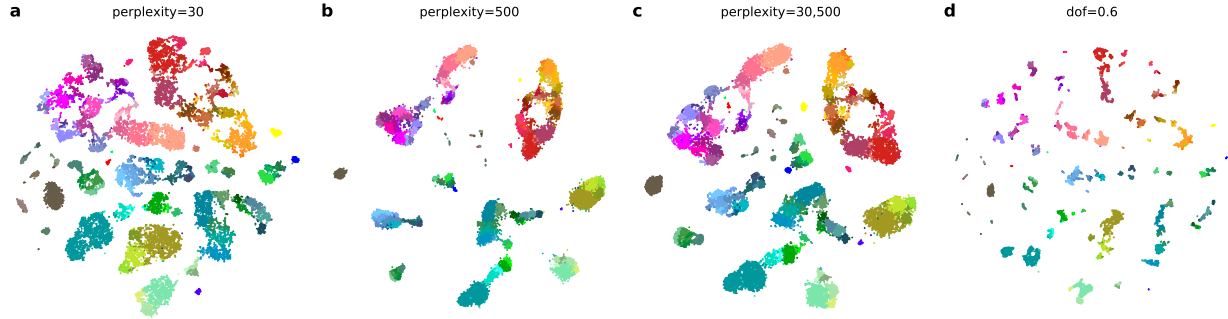


Figure 2: We use `openTSNE` to create four different visualizations of the Tasic *et al.* [5] data, each providing a different perspective into the topology of the data. The data set contains 21,874 single-cells originating from the mouse neocortex. Cluster annotations and colors are taken from the original publication. Warm colors correspond to excitatory neurons, cool colors correspond to inhibitory neurons, and gray/brown colors correspond to non-neuronal cells. Standard t-SNE (a) emphasizes local structure while increasing perplexity (b) results in a more meaningful layout of the clusters. We can also combine the two perplexities by using a multiscale kernel affinity model (c) and obtain a trade-off between global and local structure. Alternatively, we can inspect more fine-grained structure and reveal smaller clusters by using a more heavy-tailed kernel (d).

to be found through optimization [15]. `openTSNE` is currently the only publicly available library allowing users to add new samples to existing embeddings in a principled manner.

Figs. 1.b and 1.c demonstrate how we can use a previously labeled single-cell data set and embed cells from a separate experiment into the reference landscape. The reference data from Macosko *et al.* [3] contains gene expression profiles from mouse retinal cells. By embedding the samples from a similar experiment on bipolar retinal cells by Shekhar *et al.* [10], we can correctly map the bipolar cell clusters onto the reference embedding.

Embedding single cells into existing reference atlases can also be useful for cell-type classification in cases of unknown cell identities. For instance, in Fig. 4, we construct a reference embedding using labeled data from Hochgerner *et al.* [23] containing gene-expression profiles of cells from the mouse brain. The authors assign a type to each cell. We can verify their classification accuracy by visualizing the expression of well-established gene markers for the ma-

jor cell types. We then embed cells from Harris *et al.* [24] into the constructed cell atlas. In Harris *et al.*, labels are provided only for neuronal cells. In the resulting mapping, we can quickly identify other non-neuronal cell types, including oligodendrocytes and astrocytes. We can further use marker genes to validate that the mapping in the reference landscape is correct.

The examples presented above demonstrate how to use `openTSNE` to quickly gain insight into newly-sequenced, single-cell data sets by utilizing existing cell atlases. The approach is general and not limited to single-cell gene expression, and one can, in principle, apply it to any tabular data set regardless of field.

## Versatility

Versatility, the ability to use and combine different optimization approaches to construct different embedding spaces, is another of `openTSNE`'s core design principles. Kobak & Berens recently provided sev-

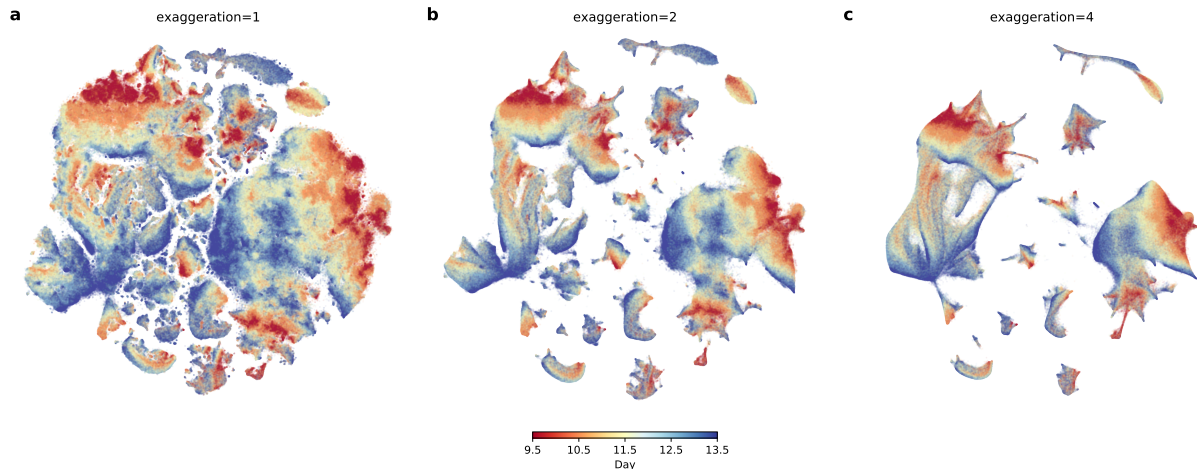


Figure 3: Increasing the exaggeration parameter leads to compact clusters, highlighting the data’s global organization and emphasizing the continuous nature of cell state transitions. The data set from Cao *et al.* [4] contains expression profiles from 2,058,652 single cells. The data were collected from mice embryos at different developmental stages at daily intervals after 9.5 to 13.5 days. (c) reveals that the data is comprised of two main components – the neural tube and mesenchymal cells – as well as several other smaller clusters. The colors indicate developmental progression with red indicating least-developed cells and blue indicating most developed cells. The overall developmental trajectory is most apparent with higher exaggeration levels, showing red cells slowly transitioning into blue cells. Progressively easing the exaggeration factor uncovers finer clusters within the larger groups, as shown in (b) with exaggeration of two and subsequently in (a), where we show the standard t-SNE with no exaggeration. 32,011 putative doublets are excluded from the visualizations.

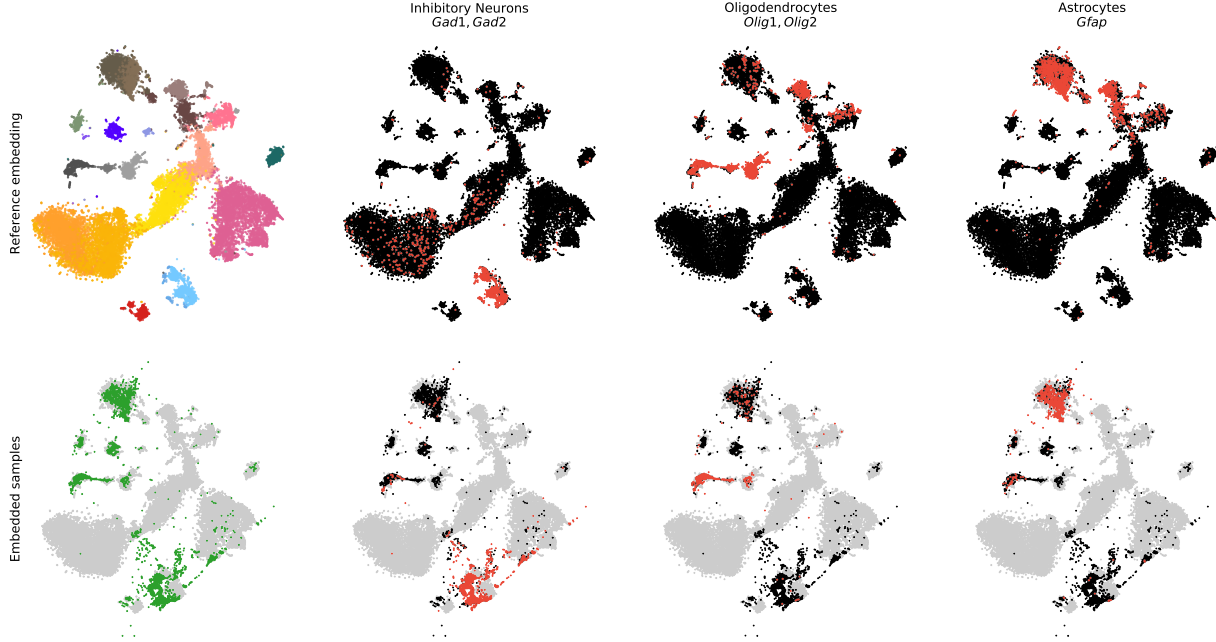


Figure 4: openTSNE supports embedding new samples into an existing reference t-SNE landscape. For the series of visualizations shown in this figure, we first construct a t-SNE embedding for the data from Hochgerner *et al.* [23] containing 24,185 developing, single cells from the mouse hippocampus. The data contains gene expression in different neurons, supporting glia, and other vascular cells (upper left). Data points representing cells are colored according to cell-types assigned in the original publication; see the legend from Fig. 2 to map colors to cell-type. We then embed new, hippocampal cells collected in a study by Harris *et al.* [24] using the embedding of Hochgerner *et al.* data as a reference. In their study, Harris *et al.* collected 6,971 single-cells and focused on identifying different types of inhibitory neurons. However, almost half of the collected cells are not neurons and were left uncharacterized. Inspecting the embeddings of these cells in the reference embedding (bottom left) reveals that in addition to inhibitory neurons, the data contains several supporting glial cells as well as a small population of endothelial cells. We can verify our approach’s accuracy by inspecting marker genes for the major cell types in the reference (top row) and embedded samples (bottom row).

eral recommendations and tricks to obtain better and more meaningful t-SNE visualizations [14]. These include multi-scale similarity kernels, perplexity annealing, and increasing exaggeration when working with massive data sets. `openTSNE` provides a flexible program interface to incorporate these improvements in just a few lines of code. Furthermore, `openTSNE` supports custom affinity models, enabling users to construct t-SNE embeddings on non-tabular relational data: the only requirement imposed by the affinity-model is some notion of similarity between data points. Finally, `openTSNE`'s comprehensive callback system can be utilized to monitor and adapt different stages of the optimization phase and has been used to construct visually appealing animations of the t-SNE optimization process.

## Speed

One of the t-SNE's common criticisms is limited scalability to large data sets containing, for instance, millions of data points [12]. The culprit for slow response time stems from a particular optimization procedure and its specific implementation in popular Python libraries. Until quite recently, most popular implementations of t-SNE were based on the Barnes-Hut approximation scheme developed by van der Maaten in 2014 [16] with asymptotic time complexity  $\mathcal{O}(N \log N)$ , where  $N$  is the number of data items (*e.g.* cells). The most widely-used implementation of t-SNE came from `scikit-learn`, which exhibits long runtimes when compared to its C++ counterpart – `MulticoreTSNE`. The multi-threaded `MulticoreTSNE` implementation [25] can construct t-SNE embeddings of millions of data points in a matter of hours on widely-accessible, consumer-grade processors (Fig. 5). However, recently, Linderman *et al.* developed a new approximation scheme – `FIt-SNE` – which further reduces the asymptotic time complexity to  $\mathcal{O}(N)$ . We include this approach in `openTSNE` enabling the embedding of large data sets in a matter of minutes.

Fig. 5 benchmarks four popular Python t-SNE implementations, including those from `scikit-learn` (v0.23.1), `MulticoreTSNE` (v0.1), `FIt-SNE` (v1.1.0), and our `openTSNE` (v0.4.3). We perform benchmarks on two computational platforms, one representing

the usage on a personal computer and the other the utility of these libraries on a high-performance computing platform. The Intel(R) Core i7 is commonly found in consumer-grade laptop computers, while Intel(R) Xeon(R) processors appear in high-performance computing machines. Benchmarks were run for 1,000 iterations with the original t-SNE parameters, as some implementations do not allow their modification.

Benchmark results (Fig. 5) confirm that both `FIt-SNE` and `openTSNE` scale better than their Barnes-Hut counterparts – `scikit-learn` and `MulticoreTSNE`. While `openTSNE`'s implementation uses Python that incurs some runtime overhead compared to its C++ counterpart `FIt-SNE`, the two libraries' speeds are surprisingly comparable. Modern computer processors contain multiple cores, allowing us to use multi-threading, which further reduces the gap between `openTSNE` and `FIt-SNE`. On the server-grade processor, `openTSNE` is slightly faster than its pure C++ counterpart when utilizing multiple cores. `openTSNE` uses `numpy` for most linear algebra operations, which may make better use of the Intel Math Kernel Library (MKL), which is aggressively optimized on Intel(R) Xeon(R) processors.

`openTSNE` provides a flexible API, allowing splitting up the embedding-construction process into several parts, caching slow operations. Running t-SNE optimization in stages enables users to quickly experiment with different parameter settings and iterate on their final visualizations.

## Ease of Use

Intuitive access and simple installation procedures almost universally correlate with the widespread adoption of novel computational techniques. While the t-SNE implementation from `scikit-learn` fits this requirement, the implementation proves prohibitively slow for even moderately-sized data sets that span tens of thousands of data records. Other C++ implementations such as `MulticoreTSNE` and `FIt-SNE` exhibit better scaling in more massive data sets, but do not provide precompiled binaries and require users to compile the software themselves. This problem is critical, for instance, for users of the Windows oper-

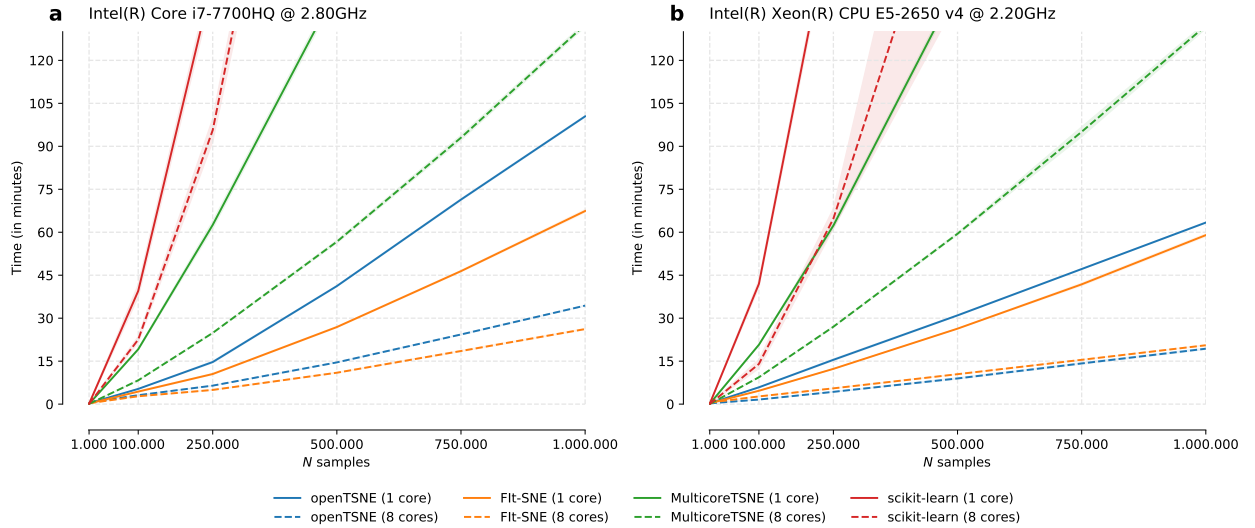


Figure 5: We benchmark `openTSNE` (v0.4.3) against three popular open-source implementations from `scikit-learn` [26] (v0.23.1), `MulticoreTSNE` [25] (v0.1), and `Flt-SNE` [13] (v1.1.0). Experiments were run on a consumer-grade Intel Core i7-7700HQ processor found in laptop computers, and on a server-grade Intel Xeon E5-2650. To generate benchmark data sets of different sizes, we subsampled data from the 10X Genomics 1.3 million mouse brain data set five times, resulting in five different data sets for each size. In total, we run each implementation on 30 different data sets. Notice that `openTSNE` scales similarly to `Flt-SNE`, as they both use the same interpolation-based approximation scheme, while `scikit-learn` and `MulticoreTSNE` utilize the Barnes-Hut approximation.

ating system, where the C++ compiler does not come with the system, making the correct configuration of current t-SNE implementations cumbersome.

We designed `openTSNE` to be accessible to a broader audience. We provide precompiled binaries for all major Python versions on all major platforms, making the installation process as seamless as possible. One can install `openTSNE` through the Python Package Index (PyPI) or `conda` from the `conda-forge` channel, the two most widely adopted Python package managers. `openTSNE`'s interface is inspired by `scikit-learn`, which is well established in the Python data science ecosystem. `openTSNE` implements multi-threaded versions of both the Barnes-Hut and FIt-SNE approximation schemes, enabling it to be applied to data sets containing millions of data points. While the Python virtual machine inevitably introduces some performance overhead, the runtime is comparable to its C++ counterpart – FIt-SNE. Finally, `openTSNE` is extensible. Its modular design enables researchers to quickly experiment with different parameter settings and easily incorporate custom components into the software. We provide a full feature list and comparison to other popular t-SNE implementations in Table 1.

## Conclusion

Text for this section ...

## Methods

This section is meant to familiarize the reader with the t-SNE algorithm and its recent extensions. We motivate each extension and introduce standard notation. This brief review is by no means comprehensive, but is self-contained and introduces the mathematics upon which the `openTSNE` library is based.

## Preliminaries

t-distributed stochastic neighbor embedding (t-SNE) is a non-linear dimensionality reduction method, which aims to find a low-dimensional embedding, where local neighborhoods are preserved. More formally, given a multi-dimensional data set  $\mathbf{X} = \{\mathbf{x}_1, \mathbf{x}_2, \dots, \mathbf{x}_N\} \in \mathbb{R}^D$  where  $N$  is the number of data points in the data set, t-SNE aims to find a low dimensional embedding  $\mathbf{Y} = \{\mathbf{y}_1, \mathbf{y}_2, \dots, \mathbf{y}_N\} \in \mathbb{R}^d$  where  $d \ll D$ , such

Table 1: We compare features of `openTSNE` to three popular open-source implementations from `scikit-learn` (v0.23.1), `MulticoreTSNE` (v0.1), and `FIt-SNE` (v1.1.0). The first section of the comparison addresses packaging and distribution. A properly packaged library is easily accessible to users, and developers should easily include it in dependency lists of other software packages. The second section of the comparison lists the two existing t-SNE approximation schemes. The FIt-SNE approximation scheme is required for t-SNE to scale up to millions of data points. The final section provides a list of extensions and improvements to the standard t-SNE algorithm, many of which can produce markedly better visualizations.

	scikit-learn	MulticoreTSNE	FIt-SNE	openTSNE
PyPI package	✓	✓	✓	
conda package	✓		✓	
Precompiled binaries	✓		✓	
Barnes-Hut ( $\mathcal{O}(N \log N)$ )	✓	✓	✓	
FIt-SNE ( $\mathcal{O}(N)$ )		✓	✓	
Multiscale Gaussian kernels		✓	✓	
Fully-custom affinity kernels			✓	
Variable degrees of freedom	✓	✓		
Variable exaggeration	✓	✓		
Better initialization	✓	✓		
Automatic learning rate	✓	✓		
Embedding new samples			✓	

that if points  $\mathbf{x}_i$  and  $\mathbf{x}_j$  are close in the high-dimensional space, their corresponding embeddings  $\mathbf{y}_i$  and  $\mathbf{y}_j$  are also close. Since t-SNE is primarily used as a visualization tool,  $d$  is typically set to two. The similarity between two data points in the high-dimensional space is defined as

$$p_{j|i} = \frac{\exp\left(-\frac{1}{2}\mathcal{D}(\mathbf{x}_i, \mathbf{x}_j)/\sigma_i^2\right)}{\sum_{k \neq i} \exp\left(-\frac{1}{2}\mathcal{D}(\mathbf{x}_i, \mathbf{x}_k)/\sigma_i^2\right)}, \quad p_{i|i} = 0 \quad (1)$$

where  $\mathcal{D}$  is some distance measure. This is then symmetrized to

$$p_{ij} = \frac{p_{j|i} + p_{i|j}}{2N}. \quad (2)$$

The bandwidth of each Gaussian kernel  $\sigma_i$  is selected such that the perplexity of the distribution matches a user-specified parameter value

$$\text{Perplexity} = 2^{H(P_i)} \quad (3)$$

where  $H(P_i)$  is the Shannon entropy of  $P_i$ ,

$$H(P_i) = -\sum_i p_{j|i} \log_2(p_{j|i}). \quad (4)$$

Different bandwidths  $\sigma_i$  enable t-SNE to adapt to the varying density of the data in the multi-dimensional space. Perplexity is sometimes interpreted as the continuous analog to the number of nearest neighbors to which distances will attempt to be preserved.

The similarity between points  $\mathbf{y}_i$  and  $\mathbf{y}_j$  in the embedding space is defined using the  $t$ -distribution with a single degree of freedom (Cauchy kernel)

$$q_{ij} = \frac{(1 + \|\mathbf{y}_i - \mathbf{y}_j\|^2)^{-1}}{\sum_{k \neq l} (1 + \|\mathbf{y}_k - \mathbf{y}_l\|^2)^{-1}}, \quad q_{ii} = 0. \quad (5)$$

The Kullback-Leibler (KL) divergence is used as a measure of agreement between distributions  $\mathbf{P}$  and  $\mathbf{Q}$

$$C = \text{KL}(\mathbf{P} \parallel \mathbf{Q}) = \sum_{ij} p_{ij} \log \frac{p_{ij}}{q_{ij}}. \quad (6)$$

The objective is to find embeddings  $\mathbf{Y}$  such that the KL divergence is minimized.

The corresponding gradient takes the form

$$\frac{\partial C}{\partial \mathbf{y}_i} = 4 \sum_{j \neq i} (p_{ij} - q_{ij}) (\mathbf{y}_i - \mathbf{y}_j) w_{ij}, \quad (7)$$

where  $w_{ij} = (1 + \|\mathbf{y}_i - \mathbf{y}_j\|^2)^{-1}$  and represents the unnormalized  $q_{ij}$ .

Optimization is performed with batch gradient descent using the delta-bar-delta update rule [27]. Originally, t-SNE was run for 1000 iterations consisting of two phases: in the first *early exaggeration* phase, the attractive forces between data

points are increased by some factor  $\rho$ , typically set to 12, so that points in the embedding can more easily move throughout the space and find their respective neighbors. The remaining 750 iterations are run with  $\rho = 1$ , which reverts the attractive forces to their original values and produces the final embedding.

Belkina *et al.* later found that faster convergence can be achieved by increasing the learning rate to  $\eta = N/12$  [19]. As a side-effect, embeddings converge faster, and the number of iterations can be lowered to 750, decreasing the overall runtime. This convention has been adopted by most modern t-SNE implementations.

## Efficient Approximation Schemes

A direct evaluation of t-SNE gradients requires  $\mathcal{O}(N^2)$  operations, which makes its application impractical to any reasonably-sized data set and beckons for the development of efficient approximation schemes. Van der Maaten observed that the t-SNE gradient may be cast as an N-body problem where data points represent particles which attract and repel each other [16]. The gradient from Eqn. (7) can be rewritten as

$$\frac{\partial C}{\partial \mathbf{y}_i} = 4 \left[ \sum_{j \neq i} p_{ij} q_{ij} Z(\mathbf{y}_i - \mathbf{y}_j) - \sum_{j \neq i} q_{ij}^2 Z(\mathbf{y}_i - \mathbf{y}_j) \right], \quad (8)$$

where  $Z = \sum_{k \neq l} (1 + \|\mathbf{y}_k - \mathbf{y}_l\|^2)^{-1}$ . This equation can then be viewed as a particle simulation, where the two terms represent the attractive and repulsive forces between individual particles. Each term lends itself to efficient approximations, which enable us to greatly reduce the time complexity of t-SNE.

## Attractive Forces

Van der Maaten observed that evaluating the attractive forces between all pairs of data points is excessive, and that considering only a handful of nearest neighbors at each point is sufficient to obtain a good approximation [16]. Because distances are transformed to similarities using a Gaussian kernel, and the bandwidth of each kernel is selected such that only a predefined number of neighbors fall within the main probability mass of the bell curve through the perplexity parameter, the remaining data points fall into the exponentially decaying tails of each Gaussian distribution. These data points are assigned near-zero probabilities and do not contribute to the overall attractive forces of data points. Therefore it is sufficient to calculate the attractive forces for only a small number of nearest neighbors instead of all  $N$  points. By utilizing tree-based nearest-neighbor search methods, the time complexity is thus reduced to  $\mathcal{O}(N \log N)$ . Linderman *et al.* further realized that, qualitatively, embeddings are visually indistinguishable when using only *approximate* nearest neighbors, further reducing time complexity to  $\mathcal{O}(N)$  [13].

## Repulsive Forces

Examining the second term of Eqn. (8) we notice that each point indiscriminately exerts a repulsive force on all other points. Van der Maaten proposed an approach based on N-body simulations and used a space-partitioning Barnes-Hut tree approach to approximate the interaction between data points [16]. Briefly, in the 2D case, the approach splits the space into quadrants and entire regions may be summarized by simple statistics. If a query point is far away from a given quadrant, the repulsive forces exerted by all the points in that quadrant onto the query point are summarized by a single point. This reduces the time complexity from  $\mathcal{O}(N^2)$  to  $\mathcal{O}(N \log N)$ .

More recently, Linderman *et al.* proposed an alternative approach, FIt-SNE, based on non-uniform convolutions for calculating all pairwise interactions between repelling data points [13]. Briefly, Linderman *et al.* observed that the repulsive forces  $\mathbf{R}$  from Eqn. (8) may be rewritten as

$$\begin{aligned} \mathbf{R}_i &= \sum_{j \neq i} q_{ij}^2 Z(\mathbf{y}_i - \mathbf{y}_j) \\ &= \sum_{j \neq i} \frac{\mathbf{y}_i - \mathbf{y}_j}{(1 + \|\mathbf{y}_i - \mathbf{y}_j\|^2)^2} / \sum_{k \neq i} \frac{1}{1 + \|\mathbf{y}_k - \mathbf{y}_i\|^2} \end{aligned} \quad (9)$$

and computed by evaluating three terms

$$\begin{aligned} \phi_{1,j} &= \sum_{j \neq i} \frac{1}{1 + \|\mathbf{y}_j - \mathbf{y}_i\|^2}, \\ \phi_{2,j} &= \sum_{j \neq i} \frac{\mathbf{y}_j}{(1 + \|\mathbf{y}_j - \mathbf{y}_i\|^2)^2}, \\ \phi_{3,j} &= \sum_{j \neq i} \frac{1}{(1 + \|\mathbf{y}_j - \mathbf{y}_i\|^2)^2}. \end{aligned} \quad (10)$$

Then the numerator and denominator of Eqn. (9) can be computed as  $\mathbf{y}_i \phi_{1,j} - \phi_{2,j}$  and  $Z = \sum_j \phi_{3,j}$ , respectively. These interactions are calculated by interpolating the terms through a grid of equispaced interpolation points. This shifts the computational burden onto the interpolation points and reduces the time complexity to  $\mathcal{O}(N)$ .

## Embedding New Samples

t-SNE is non-parametric and does not define an explicit mapping from the high-dimensional space to the embedding space. Therefore embeddings of new data points need to be found through the use of optimization techniques [15]. When adding new data points to an existing, reference embedding, the reference data points are fixed in place while new data points are allowed to find their respective positions. The optimization remains the same as in standard t-SNE with only slight

modifications to  $p_{ij}$  and  $q_{ij}$

$$p_{j|i} = \frac{\exp(-\frac{1}{2}\mathcal{D}(\mathbf{x}_i, \mathbf{v}_j)/\sigma_i^2)}{\sum_i \exp(-\frac{1}{2}\mathcal{D}(\mathbf{x}_i, \mathbf{v}_j)/\sigma_i^2)}, \quad (11)$$

$$q_{j|i} = \frac{(1 + \|\mathbf{y}_i - \mathbf{w}_j\|^2)^{-1}}{\sum_i (1 + \|\mathbf{y}_i - \mathbf{w}_j\|^2)^{-1}}, \quad (12)$$

where  $\mathbf{V} = \{\mathbf{v}_1, \mathbf{v}_2, \dots, \mathbf{v}_M\} \in \mathbb{R}^D$  where  $M$  is the number of samples in the new data set and  $\mathbf{W} = \{\mathbf{w}_1, \mathbf{w}_2, \dots, \mathbf{w}_M\} \in \mathbb{R}^d$ . Additionally, we omit the symmetrization step in Eqn. (2). Plugging these terms into Eqn. (6), we obtain the following gradient

$$\frac{\partial C}{\partial \mathbf{w}_j} = 2 \sum_i (p_{j|i} - q_{j|i}) (\mathbf{y}_i - \mathbf{w}_j) (1 + \|\mathbf{y}_i - \mathbf{w}_j\|^2)^{-1}. \quad (13)$$

Similarly to standard t-SNE, a direct calculation of gradients takes  $\mathcal{O}(N \cdot M)$  time, but it is straightforward to adapt the Barnes-Hut and FIt-SNE approximation schemes, reducing the time complexity to  $\mathcal{O}(M \log N)$  and  $\mathcal{O}(\max\{N, M\})$ , respectively. In the FIt-SNE approximation scheme, we additionally exploit the fact that the reference embedding remains fixed throughout the optimization of newly added points, and precompute the interpolation grid. This further reduces the runtime complexity from  $\mathcal{O}(\max\{N, M\})$  to  $\mathcal{O}(M)$ .

## Alternative Perplexity Kernels

In standard t-SNE, distances are converted to similarities through the use of Gaussian kernels of varying bandwidths. The bandwidths are indirectly determined by the user-specified perplexity parameter so that a fixed number of nearest data points will be assigned non-zero values. One common trick for uncovering the global relations between clusters is to increase perplexity so that more long-range interactions are preserved in the final embedding. However, one unfortunate side effect of increasing perplexity is that smaller clusters get absorbed into larger ones.

Kobak & Berens suggest that replacing the Gaussian kernel with a mixture of Gaussians may provide better insight into both the local and global structure [14]. For instance, the similarities between data points in the input space may instead be computed with

$$\begin{aligned} p_{j|i} &\propto \frac{1}{\sigma_{1,i}} \exp(-\mathcal{D}(\mathbf{x}_i, \mathbf{x}_j)/2\sigma_{1,i}^2) \\ &+ \frac{1}{\sigma_{2,i}} \exp(-\mathcal{D}(\mathbf{x}_i, \mathbf{x}_j)/2\sigma_{2,i}^2). \end{aligned} \quad (14)$$

The bandwidth of each Gaussian  $\sigma_{1,i}$  and  $\sigma_{2,i}$  is determined by selecting different perplexity values. Using a kernel with perplexity 500 captures long-range interactions which preserve

global cluster organization. Combining these with a more narrow kernel with perplexity 50 prevents small, well-defined clusters from being absorbed into larger ones, leading a better overall snapshot into the data structure.

## Variable Degrees of Freedom

Standard t-SNE reveals the clustering structure at a single level of resolution. Different perplexity parameter values can be used to identify global cluster relationships or small, well-isolated groups. Unfortunately, varying perplexity values can be time-consuming as this involves recomputing the  $k$ -nearest neighbor graph which is often the most expensive part of the t-SNE algorithm. Alternatively, Kobak *et al.* suggest that varying the degree of freedom in the t-distribution can be used to explore the clustering structure at different levels of resolution [18].

Standard t-SNE models similarities between data points in the embedding space using a t-distribution with a single degree of freedom, but this can be generalized to allow for any parameter value

$$q_{ij} \propto (1 + \|\mathbf{y}_i - \mathbf{y}_j\|^2/\alpha)^{-\alpha} = \frac{1}{(1 + \|\mathbf{y}_i - \mathbf{y}_j\|^2/\alpha)^\alpha}. \quad (15)$$

In standard t-SNE  $\alpha = 1$  so this simplifies to the Cauchy kernel from Eqn. (5). The gradient of the loss function then becomes

$$\frac{\partial C}{\partial \mathbf{y}_i} = 4 \sum_{j \neq i} (p_{ij} - q_{ij}) w_{ij}^{1/\alpha} (\mathbf{y}_i - \mathbf{y}_j), \quad (16)$$

which can, again, be cast as the interplay between the attractive and repulsive forces between particles

$$\begin{aligned} \frac{\partial C}{\partial \mathbf{y}_i} &= 4 \sum_{j \neq i} p_{ij} w_{ij}^{1/\alpha} (\mathbf{y}_i - \mathbf{y}_j) \\ &\quad - 4 \sum_{j \neq i} w_{ij}^{\frac{\alpha+1}{\alpha}} / Z(\mathbf{y}_i - \mathbf{y}_j). \end{aligned} \quad (17)$$

Adapting existing approximation schemes to this formulation is straightforward. `openTSNE` provides efficient implementations of both the Barnes-Hut and the FIt-SNE approximation schemes, where we modify the terms from Eqn. (10) to

$$\begin{aligned} \phi_{1,j} &= \sum_{j \neq i} \frac{1}{(1 + \|\mathbf{y}_j - \mathbf{y}_i\|^2/\alpha)^{\alpha+1}}, \\ \phi_{2,j} &= \sum_{j \neq i} \frac{\mathbf{y}_j}{(1 + \|\mathbf{y}_j - \mathbf{y}_i\|^2/\alpha)^{\alpha+1}}, \\ \phi_{3,j} &= \sum_{j \neq i} \frac{1}{(1 + \|\mathbf{y}_j - \mathbf{y}_i\|^2/\alpha)}. \end{aligned}$$

## Variable Exaggeration

Embeddings produced by standard t-SNE often produce clusters separated by thin boundaries and make use of all available space. While this is desirable at times, it often obscures the global relationships between clusters as all neighboring clusters appear about the same distance from one another. Other dimensionality reduction methods such as UMAP [2] or ForceAtlas2 [21] tend to produce embeddings where clusters appear more compact and the white-space separating the clusters may be interpreted at least partially as a loose measure of distance.

Böhm *et al.* showed that the exaggeration factor  $\rho$  can be used to produce layouts more similar to UMAP and ForceAtlas2 [22]. By incorporating exaggeration into later phases of optimization, t-SNE is able to introduce more white-space between clusters which better reflects the global relations between clusters. Böhm *et al.* found that using  $\rho = 4$  and  $\rho = 30$  produces embeddings visually similar to UMAP and ForceAtlas2, respectively.

While it is difficult to claim one is better than the other, different settings of  $\rho$  may uncover different properties of the data manifold. For example, in single-cell data, standard t-SNE often uncovers distinct, well-separated groups of cell-types but obscures transitional paths between cell-states. This problem is exacerbated when dealing with large numbers of data points. On the other hand, ForceAtlas2 has been used successfully to uncover trajectories and transitions between cell types. Unfortunately, when using ForceAtlas2, large clusters often absorb small, distinct groups of cells. One might run t-SNE with various parameter settings to avoid switching between different algorithms and obtain similar visualizations. We might generate an embedding using higher levels of exaggeration to highlight the developmental transitions between cell types and one with low levels of exaggeration to identify clear populations of cells.

## Globally Consistent Initialization Schemes

t-SNE, UMAP, and ForceAtlas2 can all be cast as force-directed layout algorithms, which operate on the  $k$ -nearest neighbor graph. Each method constructs the graph differently and specifies the attractive and repulsive forces in its own way, but ultimately, point positions are found by balancing the attractive and repulsive forces between data points.

The final positions of data points in this class of algorithms is largely dependent on the embedding initialization. UMAP found early success as it was able to produce visualizations that better captured the global organization of clusters. This was due to its initialization scheme, which initialized point positions using Laplacian eigenmaps. On the other hand, most implementations of t-SNE performed random initialization, which resulted in poor global coherence. However, Kobak & Linderman recently showed that using the same initialization for both methods leads to visualizations, which exhibit similarly good global coherency. Conversely, when initialized

randomly, both methods produce visualizations where clusters are arbitrarily positioned in the embedding space.

`openTSNE` defaults to using the two leading principal components as initialization, but also provides a spectral approach similar to UMAP. This allows clusters in resulting embeddings to be organized in a more globally coherent manner, leading to increased visualization interpretability.

## Availability

`openTSNE` is distributed under the BSD-3-Clause License and is publicly available as an open-source package at <https://github.com/pavlin-policar/openTSNE>. `openTSNE` is also available on PyPI and conda-forge. The data sets used and scripts used in this study are included in accompanying notebooks, publicly available at <https://github.com/pavlin-policar/opentsne-paper>.

## Competing interests

The authors declare that they have no competing interests.

## Author's contributions

P.G.P. implemented and maintains `openTSNE` library. M.S. helped in development of mathematical foundations and advised on inclusion of the extensions. B.Z. initiated and supervised the project. All three co-authors wrote the manuscript.

## Acknowledgements

We want to thank Dmitry Kobak for various helpful discussions and best practices when using t-SNE and his contributions to the source code. We would also like to thank George Linderman for his help with the Fit-SNE algorithm.

## References

- [1] Van Der Maaten, L., Hinton, G.: Visualizing data using t-SNE. *Journal of Machine Learning Research* **9**(Nov), 2579–2605 (2008)
- [2] McInnes, L., Healy, J., Melville, J.: UMAP: Uniform Manifold Approximation and Projection for Dimension Reduction. *ArXiv e-prints* (2018). [1802.03426](https://arxiv.org/abs/1802.03426)
- [3] Macosko, E.Z., Basu, A., Satija, R., Nemesh, J., Shekhar, K., Goldman, M., Tirosh, I., Bialas, A.R., Kamitaki, N., Marstersteck, E.M., et al.: Highly parallel genome-wide expression profiling of individual cells using nanoliter droplets. *Cell* **161**(5), 1202–1214 (2015)
- [4] Cao, J., Spielmann, M., Qiu, X., Huang, X., Ibrahim, D.M., Hill, A.J., Zhang, F., Mundlos, S., Christiansen, L., Steemers, F.J., et al.: The single-cell transcriptional landscape of mammalian organogenesis. *Nature* **566**(7745), 496–502 (2019)
- [5] Tasic, B., Yao, Z., Graybuck, L.T., Smith, K.A., Nguyen, T.N., Bertagnolli, D., Goldy, J., Garren, E., Economo, M.N., Viswanathan, S., et al.: Shared and distinct transcriptomic cell types across neocortical areas. *Nature* **563**(7729), 72–78 (2018)
- [6] Hirata, J., Hosomichi, K., Sakaue, S., Kanai, M., Nakaoka, H., Ishigaki, K., Suzuki, K., Akiyama, M., Kishikawa, T., Ogawa, K., et al.: Genetic and phenotypic landscape of the major histocompatibility complex region in the Japanese population. *Nature Genetics* **51**(3), 470–480 (2019)
- [7] Beaulaurier, J., Zhu, S., Deikus, G., Mogno, I., Zhang, X.-S., Davis-Richardson, A., Canepa, R., Triplett, E.W., Faith, J.J., Sebra, R., et al.: Metagenomic binning and association of plasmids with bacterial host genomes using DNA methylation. *Nature Biotechnology* **36**(1), 61 (2018)
- [8] Sheth, R.U., Li, M., Jiang, W., Sims, P.A., Leong, K.W., Wang, H.H.: Spatial metagenomic characterization of microbial biogeography in the gut. *Nature Biotechnology* **37**(8), 877–883 (2019)
- [9] Tkachev, A., Stepanova, V., Zhang, L., Khrameeva, E., Zubkov, D., Giavalisco, P., Khaitovich, P.: Differences in lipidome and metabolome organization of prefrontal cortex among human populations. *Scientific Reports* **9**(1), 1–10 (2019)
- [10] Shekhar, K., Lapan, S.W., Whitney, I.E., Tran, N.M., Macosko, E.Z., Kowalczyk, M., Adiconis, X., Levin, J.Z., Nemesh, J., Goldman, M., et al.: Comprehensive classification of retinal bipolar neurons by single-cell transcriptomics. *Cell* **166**(5), 1308–1323 (2016)
- [11] Ding, J., Condon, A., Shah, S.P.: Interpretable dimensionality reduction of single cell transcriptome data with deep generative models. *Nature Communications* **9**(1), 2002 (2018)
- [12] Becht, E., McInnes, L., Healy, J., Dutertre, C.-A., Kwok, I.W., Ng, L.G., Ginhoux, F., Newell, E.W.: Dimensionality reduction for visualizing single-cell data using UMAP. *Nature Biotechnology* **37**(1), 38 (2019)
- [13] Linderman, G.C., Rachh, M., Hoskins, J.G., Steinerberger, S., Kluger, Y.: Fast interpolation-based t-SNE for improved visualization of single-cell RNA-seq data. *Nature Methods* **16**(3), 243–245 (2019)

- [14] Kobak, D., Berens, P.: The art of using t-SNE for single-cell transcriptomics. *Nature Communications* **10**(1), 1–14 (2019)
- [15] Poličar, P.G., Stražar, M., Zupan, B.: Embedding to reference t-SNE space addresses batch effects in single-cell classification. In: International Conference on Discovery Science, pp. 246–260 (2019). Springer
- [16] Van Der Maaten, L.: Accelerating t-SNE using tree-based algorithms. *The Journal of Machine Learning Research* **15**(1), 3221–3245 (2014)
- [17] Kobak, D., Linderman, G.C.: UMAP does not preserve global structure any better than t-SNE when using the same initialization. *bioRxiv* (2019)
- [18] Kobak, D., Linderman, G., Steinerberger, S., Kluger, Y., Berens, P.: Heavy-tailed kernels reveal a finer cluster structure in t-SNE visualisations. In: Joint European Conference on Machine Learning and Knowledge Discovery in Databases, pp. 124–139 (2019). Springer
- [19] Belkina, A.C., Ciccolella, C.O., Anno, R., Halpert, R., Spidlen, J., Snyder-Cappione, J.E.: Automated optimized parameters for T-distributed stochastic neighbor embedding improve visualization and analysis of large datasets. *Nature Communications* **10**(1), 1–12 (2019)
- [20] Buitinck, L., Louppe, G., Blondel, M., Pedregosa, F., Mueller, A., Grisel, O., Niculae, V., Prettenhofer, P., Gramfort, A., Grobler, J., Layton, R., VanderPlas, J., Joly, A., Holt, B., Varoquaux, G.: API design for machine learning software: experiences from the scikit-learn project. In: ECML PKDD Workshop: Languages for Data Mining and Machine Learning, pp. 108–122 (2013)
- [21] Jacomy, M., Venturini, T., Heymann, S., Bastian, M.: ForceAtlas2, a continuous graph layout algorithm for handy network visualization designed for the Gephi software. *PloS One* **9**(6), 98679 (2014)
- [22] Böhm, J.N., Berens, P., Kobak, D.: A Unifying Perspective on Neighbor Embeddings along the Attraction-Repulsion Spectrum. *arXiv preprint arXiv:2007.08902* (2020)
- [23] Hochgerner, H., Zeisel, A., Lönnberg, P., Linnarsson, S.: Conserved properties of dentate gyrus neurogenesis across postnatal development revealed by single-cell RNA sequencing. *Nature Neuroscience* **21**(2), 290–299 (2018)
- [24] Harris, K.D., Hochgerner, H., Skene, N.G., Magno, L., Katona, L., Gonzales, C.B., Somogyi, P., Kessaris, N., Linnarsson, S., Hjerling-Leffler, J.: Classes and continua of hippocampal CA1 inhibitory neurons revealed by single-cell transcriptomics. *PLoS Biology* **16**(6), 2006387 (2018)
- [25] Ulyanov, D.: Multicore-TSNE. GitHub (2016)
- [26] Pedregosa, F., Varoquaux, G., Gramfort, A., Michel, V., Thirion, B., Grisel, O., Blondel, M., Prettenhofer, P., Weiss, R., Dubourg, V., et al.: Scikit-learn: Machine learning in Python. *The Journal of Machine Learning Research* **12**, 2825–2830 (2011)
- [27] Jacobs, R.A.: Increased rates of convergence through learning rate adaptation. *Neural Networks* **1**(4), 295–307 (1988)